hep-ph/0101314

Higgs Radiation off Quarks in the Standard Model and supersymmetric Theories at e^+e^- Colliders

Michael Spira

Paul–Scherrer-Institut, CH–5232 Villigen PSI, Switzerland

Abstract

Yukawa couplings between Higgs bosons and quarks in the Standard Model (SM) and supersymmetric theories can be measured in the processes $e^+e^- \to Q\bar{Q}+$Higgs. The cross sections and Higgs energy distributions of these processes in the SM and minimal supersymmetric model have been determined including the complete set of next-to-leading order QCD corrections for all channels.

Presented at the

5th International Symposium on Radiative Corrections
(RADCOR–2000)
Carmel CA, USA, 11–15 September, 2000

1 Introduction

In the Standard Model (SM) and its supersymmetric extensions, the masses of electroweak gauge bosons, leptons, and quarks are generated by interactions with Higgs fields [1]. The Yukawa couplings between Higgs particles and fermions therefore grow with the masses M_f of the fermions. The couplings obey a universal scaling law $g_{ffH} = M_f/v$ in the SM, with $v \approx 246\,\text{GeV}$ being the ground-state value of the Higgs field. In supersymmetric models, which involve at least two Higgs doublets, the size of the Yukawa couplings is also set by the fermion masses, yet the relationship is more complex owing to the mixing among the Higgs fields. The Yukawa couplings [2] of the two CP-even light/heavy Higgs bosons h/H and of the CP-odd Higgs boson A in the minimal supersymmetric extension of the Standard Model (MSSM) [3, 4], expressed in units of the SM couplings, are determined by the parameters $\text{tg}\beta = v_2/v_1$, the ratio of the vacuum expectation values of the two Higgs fields generating the masses of up- and down-type particles, and α, the mixing angle in the CP-even sector. In the decoupling limit, in which the light Higgs mass reaches the maximum value for a given parameter $\text{tg}\beta$, the h Yukawa couplings approach the SM values. In general, they are suppressed for up-type fermions and enhanced for down-type fermions; the enhancement increases with $\text{tg}\beta$ and can therefore be very strong.

Higgs radiation off top or off bottom quarks in e^+e^- collisions,

$$e^+e^- \to Q\bar{Q}\phi \qquad [Q = t, b;\ \phi = H_{SM}, h, H, A], \tag{1}$$

lends itself as a suitable process for measuring the Yukawa couplings of all Higgs bosons [5], particularly for the SM Higgs bosons, the light Higgs boson h and for moderately heavy Higgs bosons H and A. Within the SM it has been demonstrated that the top Yukawa coupling can be measured with an accuracy of 2–3% at linear colliders with $\sqrt{s} = 800$ GeV [6]. We present the cross sections for these processes including the next-to-leading order (NLO) QCD corrections [7, 8]. In this analysis we have calculated the complete set of $\mathcal{O}(\alpha_s)$ QCD corrections to all subchannels in (1) systematically. The large number of interfering subchannels in supersymmetric theories renders this program more complex than the corresponding calculation in the SM, in particular since the relative weight of the subchannels varies over the supersymmetric parameter space and over the phase space for different mass ratios. Moreover, the Higgs-energy distributions haven been obtained at NLO [9]. They turn out to be relevant in the separation of the resonant parts and those, which depend on the Yukawa couplings. Introducing appropriate cuts in the Higgs energy the sensitivity to the Yukawa couplings can be increased experimentally.

2 QCD Corrections

The QCD corrections can be categorized into five classes. Virtual corrections of the internal quark lines, of the γ/Z–quark vertices, of the Higgs–quark vertices, and box diagrams interfere with the Born amplitude. Gluon radiation off internal and external quark lines adds incoherently to the cross sections. The value of the electromagnetic

coupling is taken to be $\alpha = 1/128$ and the Weinberg angle as $\sin^2\theta_W = 0.23$. The mass of the Z boson is set to $M_Z = 91.187\,\text{GeV}$, and the pole masses of the top and bottom quarks are set to $M_t = 174\,\text{GeV}$ [10] and[1] $M_b = 4.62\,\text{GeV}$ [11], respectively. The masses of the MSSM Higgs bosons and their couplings are related to tgβ and the pseudoscalar Higgs boson mass M_A. In the relation we use, higher-order corrections up to two loops in the effective-potential approach are included [12]. The SUSY parameters are chosen as $\mu = A_t = A_b = 0$ and $M_{\tilde{Q}} = 1$ TeV; this simple choice is sufficient to illustrate the main results.

The production of $b\bar{b}\phi$ final states can be mediated by resonance channels $e^+e^- \to ZH_{SM}, Zh, ZH$ and $e^+e^- \to Ah, AH$. We describe the resonance structures as Breit–Wigner forms by substituting $M^2 \to M^2 - iM\Gamma$ in all boson propagators. The decay widths of the Higgs bosons are calculated including higher-order corrections, as described in Refs. [13, 14], while the Z width is set to $\Gamma_Z = 2.49\,\text{GeV}$. For $t\bar{t}\phi$ production the widths can be neglected, since the Higgs masses are taken below the $t\bar{t}$ threshold. The renormalization scale of the QCD coupling α_s, which is evaluated in NLO with five active flavors normalized to $\alpha_\text{s}(M_Z^2) = 0.119$ [10], is chosen at $\mu_R^2 = s$, where $s = E_\text{CM}^2$ is the center-of-mass (CM) energy squared.

The QCD radiative corrections have been calculated in the standard way. The Feynman diagrams have been evaluated within dimensional regularization. Ultraviolet divergences are consistently regularized in $D = 4-2\epsilon$ dimensions, with γ_5 treated naively since no anomalies are involved. The renormalization of the $Q\bar{Q}\phi$ vertices is connected to the renormalization of the quark masses, which, in the case of the top quark, is defined on shell (see e.g. Refs. [15, 16] for details). In the case of bottom quarks large logarithms are mapped into the running mass $\overline{m}_b(Q^2_\text{Higgs})$ for the Yukawa couplings of the b quark, with Q^2_Higgs denoting the squared momentum flow through the corresponding Higgs-boson line. The infrared divergences encountered in the virtual corrections and in the cross section for real gluon emission, are treated in two different ways. Both calculations follow subtraction procedures, one using dimensional regularization and one introducing an infinitesimal gluon mass [17]. The results obtained by the two different procedures are in mutual numerical agreement after adding the contributions from virtual gluon exchange and real gluon emission. A second, completely independent calculation of the QCD corrections to the total cross section was based on the evaluation of all relevant cut diagrams of the photon and Z-boson self-energies in two-loop order, generalizing the method applied to $t\bar{t}(g)$ intermediate states in Ref. [18]. The results of the two approaches are in numerical agreement. Moreover, the parts that have been calculated in Refs. [19, 20], i.e. photon exchange and resonant contributions, are in full agreement with our corresponding partial results.

[1] This value for the perturbative pole mass of the bottom quark corresponds in NLO to an $\overline{\text{MS}}$ mass $\overline{m}_b(\overline{m}_b) = 4.28\,\text{GeV}$.

3 Results

a.) Asymptotic behaviour. The QCD corrections to the top final states $t\bar{t}\phi$ can be interpreted easily in two kinematical areas. Whenever the invariant mass of the $t\bar{t}$ pair is close to threshold, the gluonic Sommerfeld rescattering-correction is positive and becomes large. In the threshold region the K factor approaches the asymptotic form [7]

$$K_{\rm thr}^{t\bar{t}\phi} \to 1 + \frac{32\alpha_s}{9\beta_t} \tag{2}$$

with the maximal quark velocity $\beta_t = \sqrt{(\sqrt{s} - M_\phi)^2 - 4M_t^2}/2M_t$ in the $(t\bar{t})$ rest frame.

For high energies, on the other hand, the QCD corrections are of order α_s/π. In the energy region $s \gg 4M_t^2 \gg M_H^2$ but $\log s/M_t^2 \not\gg \mathcal{O}(1)$, which is relevant for the present analysis, the QCD corrections can qualitatively be traced back to vertex corrections and infrared gluon radiation. Since scalar Higgs bosons are radiated off top quarks preferentially with small energy $[x = E_\phi/E_t \to 0]$, as is evident from the leading (universal) part of the fragmentation function

$$f(t \to tH; x) = \frac{g_{ttH}^2}{16\pi^2}\left[4\ \frac{1-x}{x} + x\ \log\frac{s}{M_t^2}\right]\ , \tag{3}$$

the QCD correction of the scalar Yukawa vertex, regularized by soft gluon radiation, approaches the value [19]

$$\Delta_H^{V+IR} = \frac{4\alpha_s}{3\pi}\left[-1 + \frac{2-x}{x}\log(1-x)\right] \to -4\frac{\alpha_s}{\pi}\ . \tag{4}$$

The scalar Yukawa vertex is therefore reduced by four units in α_s/π which are compensated only partly by one unit due to the increase of the $t\bar{t}$ production probability, leading in total [7, 19] to

$$K_{\rm cont}^{t\bar{t}\phi} \to 1 - 3\frac{\alpha_s}{\pi} + \ldots \quad \text{for } \phi = H_{SM}, h, H\ . \tag{5}$$

The ellipsis accounts for hard Higgs and gluon radiation (of order $+\alpha_s/\pi$). Thus, the QCD corrections are expected negative for scalar Higgs particles in the high energy continuum.

By contrast, the corresponding fragmentation function for the pseudoscalar Higgs boson [21]

$$f(t \to tA; x) = \frac{g_{ttA}^2}{16\pi^2}\ x\ \log\frac{s}{M_t^2} \tag{6}$$

is hard so that the average of the vertex and IR gluon corrections over the Higgs spectrum amounts to

$$\Delta_A^{V+IR} \to \frac{4\alpha_s}{3\pi}\left\langle\left[1 + \frac{2-x}{x}\log(1-x)\right]\right\rangle \sim -\frac{3}{2}\frac{\alpha_s}{\pi}\ . \tag{7}$$

Adding to this correction the increase of the $t\bar{t}$ production probability of one unit, the K factor is very close to unity

$$K_{\rm cont}^{t\bar{t}A} \to 1 - \frac{1}{2}\frac{\alpha_s}{\pi} + \ldots \tag{8}$$

After hard gluon bremsstrahlung is taken into account (symbolized by the ellipsis), the overall QCD corrections for the pseudoscalar Higgs boson are therefore expected slightly positive. [For ultra-high energies, i.e. $\log s/M_t^2 \gg 1$, hard gluon bremsstrahlung becomes important. Similarly to the leading terms in the fragmentation functions eqs. (3) and (6), the QCD corrections for scalar and pseudoscalar Higgs bosons approach each other as a result of chiral symmetry restoration in *asymptotia*; this has been verified in a numerical calculation.]

Similar estimates can be applied to bottom final states which in general are dominated by resonance decays. After absorbing the large logarithms $\log(Q_\phi^2/M_b^2)$ into the Yukawa couplings, the non-leading effects are positive:

$$K_{\rm res}^{b\bar{b}\phi} \approx 1 + \left\{\tfrac{17}{3}, 1\right\} \frac{\alpha_s}{\pi} \quad \text{for } \{\text{Higgs}, Z\} \to b\bar{b} \ . \tag{9}$$

Also close to the thresholds and in the high-energy limit the QCD corrections remain positive after mapping the large (negative) corrections into the running Yukawa couplings. Since different channels are activated at the same time, only a qualitative estimate can be given in the continuum regime,

$$K_{\rm cont}^{b\bar{b}\phi} = 1 + c\frac{\alpha_s}{\pi} \quad \text{with } c = \mathcal{O}(1), \tag{10}$$

while details must be left to the numerical analysis.

b.) Numerical results. The total cross sections for $Ht\bar{t}$ production in the SM are

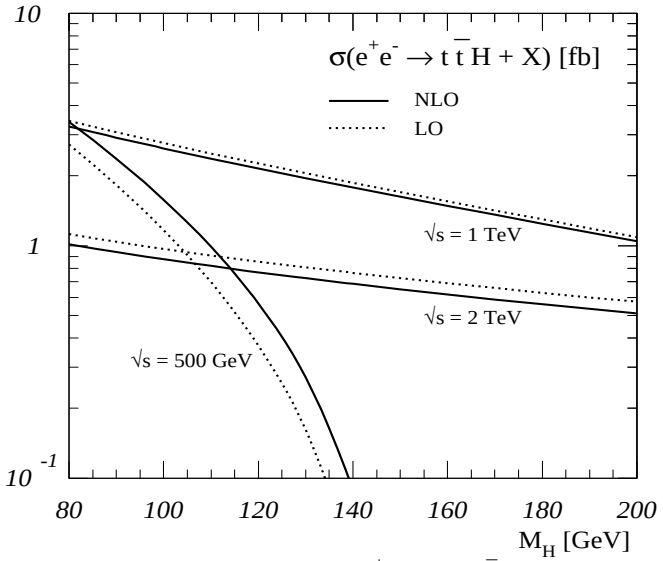

Figure 1: *The total cross section for the process $e^+e^- \to t\bar{t}H+X$, including QCD radiative corrections (full curve) and at LO (dashed curve) as a function of the scaled Higgs energy x_H [7].*

presented in Fig. 1 as a function of the Higgs mass for different collider energies [7]. The

NLO (LO) cross sections are given by the full (dotted) curves. The QCD corrections are large for $\sqrt{s} = 500$ GeV due to the Coulomb singularity at threshold and moderate for high energies. At high energies the results agree with the approximation of eq. (5). The cross sections amount to more than about 0.1 fb, which leads to a significant number of events at the TESLA collider, being designed to reach integrated luminosities of about $\int \mathcal{L} \sim 1$ ab^{-1} in three years of operation. The corresponding Higgs-energy distribution is presented in Fig. 2 for $M_H = 120$ GeV as a function of the scaled variable $x_H = 2E_H/\sqrt{s}$ [9]. The shape of the distribution is shifted towards larger values of x_H due to the Coulomb singularity at threshold. The results for small values of x_H reproduce the approximation of eq. (5).

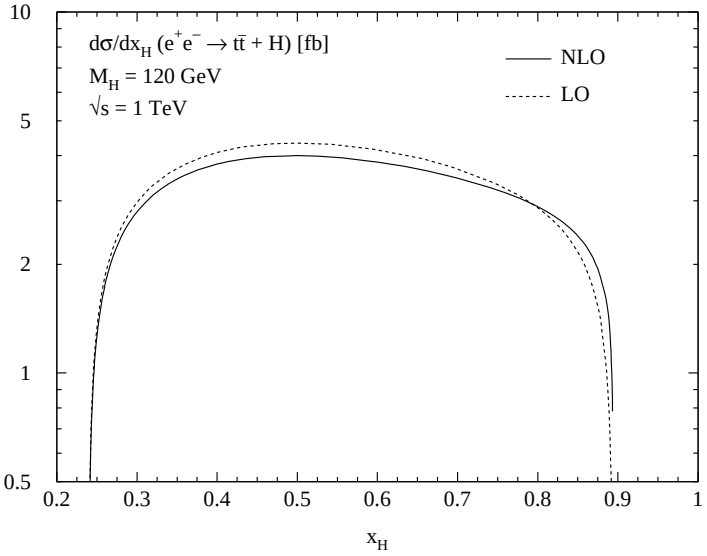

Figure 2: *The Higgs-energy distribution for the process $e^+e^- \to t\bar{t}H + X$, including QCD radiative corrections (full curve) and at LO (dashed curve) as a function of the scaled Higgs energy x_H [9].*

The results for the MSSM are exemplified in Fig. 3 for tg$\beta = 3$[2] and 30 and for the collider energy $E_{\rm CM} = 500\,{\rm GeV}$ [8]. If required by the size of the cross section, which should not fall below $\sim 10^{-2}$ fb in order to be accessible experimentally, we switched to $E_{\rm CM} = 1\,{\rm TeV}$. The Born terms are shown by the dotted curves, while the final results for the cross sections, including QCD corrections, are given by the full curves.

For $E_{\rm CM} = 500\,{\rm GeV}$ the QCD corrections to Higgs-boson production in association with $t\bar{t}$ pairs increase the scalar Higgs-production cross sections significantly, as can be inferred from Fig. 3. Close to threshold the numerical results clearly exhibit the strong increase of the cross sections due to the Coulomb singularity (2). Moreover, for tg$\beta = 30$ the cross sections are strongly suppressed except for the regions where the light (heavy)

[2]Although the value tg$\beta = 3$ is already excluded for vanishing mixing in the stop sector, this choice exemplifies the complete result for smaller values of tgβ and can easily be extended to the non-vanishing stop mixing case.

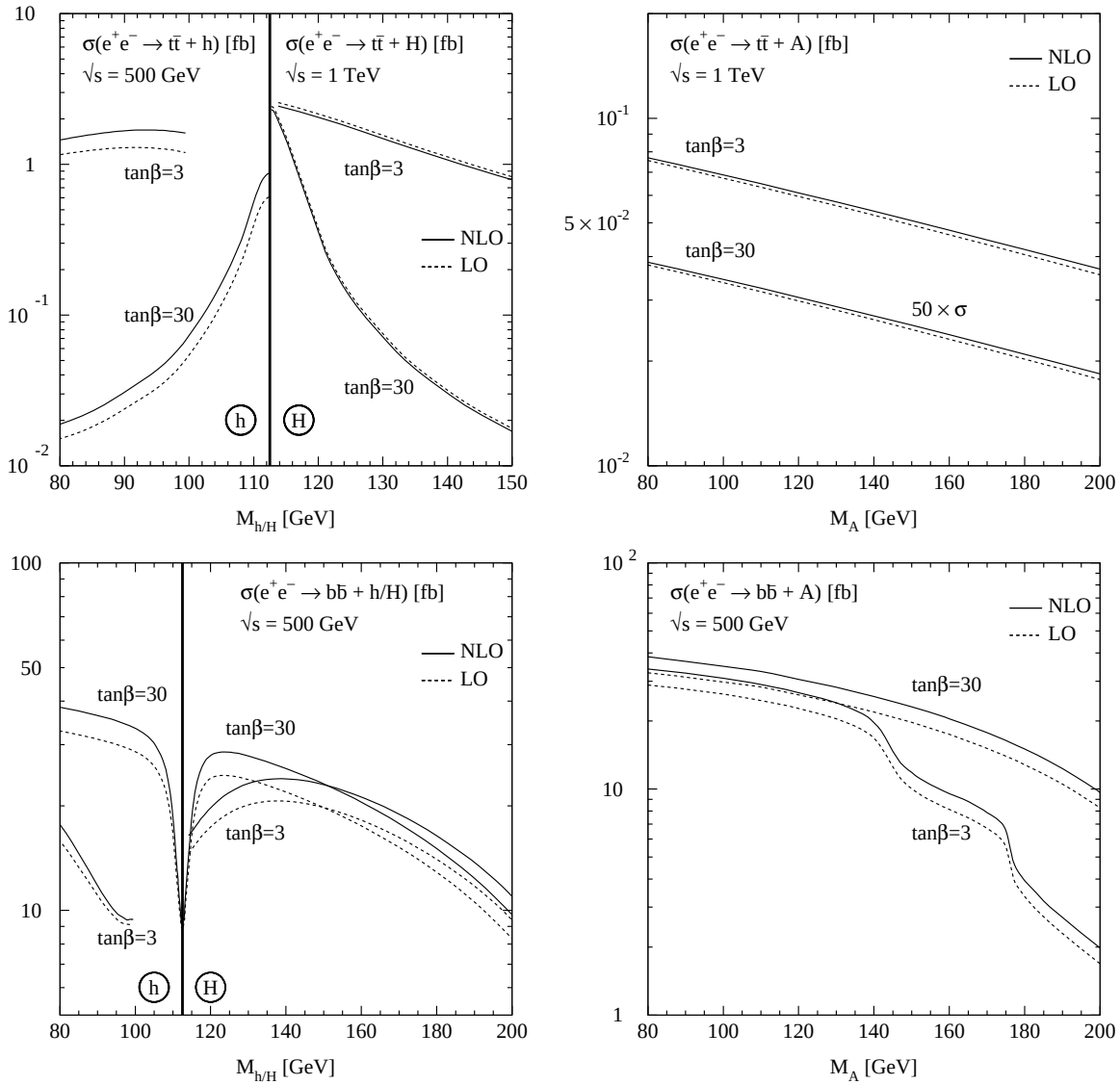

Figure 3: *Production cross sections for the MSSM Higgs bosons h, H and A in association with heavy t, b quark pairs [8]; Born approximation: dashed, QCD corrections included: full curves. The rapid drops in the $b\bar{b}A$ cross section at $tg\beta = 3$ are due to the kinematical opening of the resonant $H \to WW, hh$ decays, which reduce the branching ratio of the resonant $H \to b\bar{b}$ decay.*

scalar Higgs mass is close to its upper (lower) bound. For $\mathrm{tg}\beta = 3$ the cross section amounts to about 1 fb, which leads to a significant number of events at the TESLA collider.

For CM energies of 1 TeV the QCD corrections to scalar Higgs production in association with $t\bar{t}$ pairs are of moderate size. They decrease the cross sections by about 3–5%. This is in accordance with the asymptotic form of the K factor [7]. For pseudoscalar Higgs production, the size of the QCD corrections is slightly positive at 1 TeV, in agreement with the qualitative discussion above.

The cross sections for Higgs-boson production associated with $b\bar{b}$ pairs are significantly larger due to the resonance contributions from on-shell Z and Higgs-boson decays into $b\bar{b}$ pairs. The QCD corrections increase these cross sections by about 5–25%. The drop in the $b\bar{b}A$ production cross section for $\mathrm{tg}\beta = 3$ at $M_A \sim 140\,\mathrm{GeV}$ and 175 GeV can be attributed to the crossing of the thresholds for resonant $H \to WW$ and $H \to hh$ decays, respectively, in HA final states.

Without cuts, the intermediate resonance decays $Z, h, H, A \to b\bar{b}$ dominate all $b\bar{b}\phi$ production processes, whenever they are kinematically allowed, and it will be difficult to extract the bottom Yukawa couplings experimentally in regions where resonant Higgs decays to $b\bar{b}$ pairs are dominant. This is the case at large values of $\mathrm{tg}\beta$ for all neutral Higgs particles and at small values of $\mathrm{tg}\beta$ for Higgs masses below the WW threshold. In these cases the branching ratios, which determine the size of the $b\bar{b}\phi$ cross sections, will be nearly independent of the bottom Yukawa couplings. Resonance decays $R \to b\bar{b}$ in the $b\bar{b}h/H/A$ final states can however be eliminated by cutting out the resonance energy of the final-state Higgs boson, $E_{\phi,\mathrm{res}} = (s + M_\phi^2 - M_R^2)/2\sqrt{s}$. After subtracting these resonance parts, the non-resonant contributions are suppressed by about one to three orders of magnitude. The resonances have been removed from the cross sections in the examples of Fig. 4 by subtracting the two-particle cross sections in the Breit–Wigner bands $M_R \pm \Delta$ of the energy $E_{\phi,\mathrm{res}}$ with the resolution $\Delta = 5\,\mathrm{GeV}$. This theoretical definition is used for the sake of simplicity; wider cuts may be required in experimental analyses. Peaks and dips in the cross sections are the result of overlapping Breit-Wigner bands. For the scalar Higgs particles they arise from overlapping Z and A boson bands; in pseudoscalar Higgs production the light and heavy scalar resonance bands overlap for 100 GeV $\lesssim M_A \lesssim 120$ GeV for $\mathrm{tg}\beta = 30$. The dips occur whenever the two resonance bands touch each other, while the peaks between the dips occur when the resonance masses coincide exactly. As shown in Fig. 4, the QCD-corrected cross sections are still close to 1 fb or slightly below, except for heavy masses at small values of $\mathrm{tg}\beta$. Thus, ensembles of order 10^3 events can be collected at a high-luminosity collider [8].

Fig. 5 presents the pseudoscalar Higgs-energy distribution in $t\bar{t}A$ production at $\sqrt{s} = 1$ TeV for $M_A = 120\,\mathrm{GeV}$ and $\mathrm{tg}\beta = 3$ as a function of the scaled Higgs energy $x_A = 2E_A/\sqrt{s}$ [9]. As in the case of the SM Higgs boson the distribution is shifted towards larger Higgs energies due to the Coulomb singularity at threshold. Moreover, it is clearly visible from the comparison of Figs. 2 and 5 that the pseudoscalar energy spectrum is harder than the scalar one, which is related to the absence of the $1/x$ enhancement in eq. (6).

The corresponding Higgs-energy distributions of $b\bar{b}h$ production for $M_h = 110$ GeV is

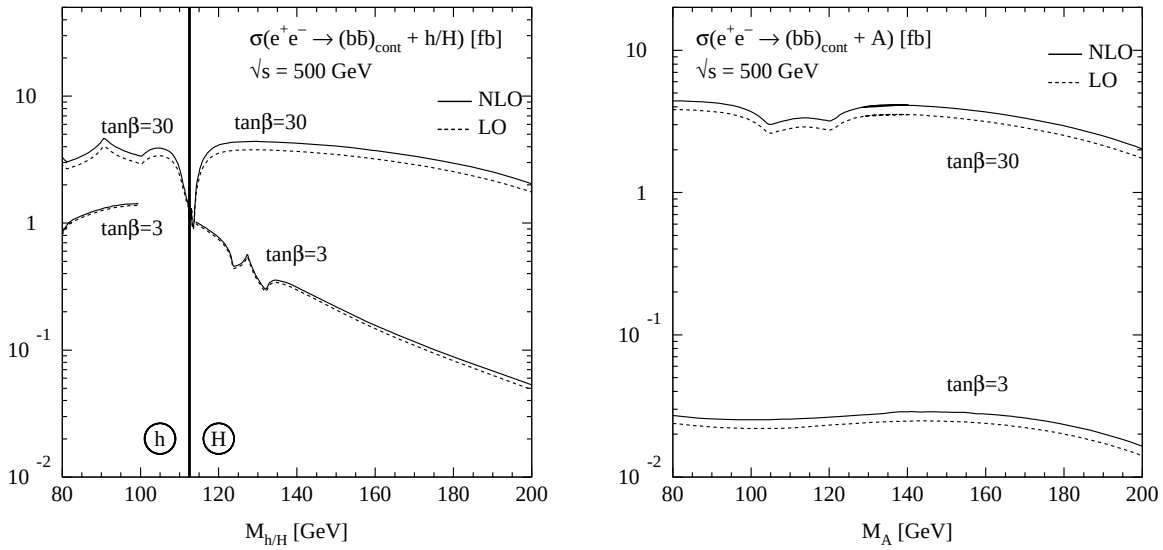

Figure 4: *Continuum production of MSSM Higgs bosons h, H, A in association with a $b\bar{b}$ pair after subtraction of resonance decays to $b\bar{b}$ pairs in the Breit-Wigner bands $M_R \pm 5$ GeV [8].*

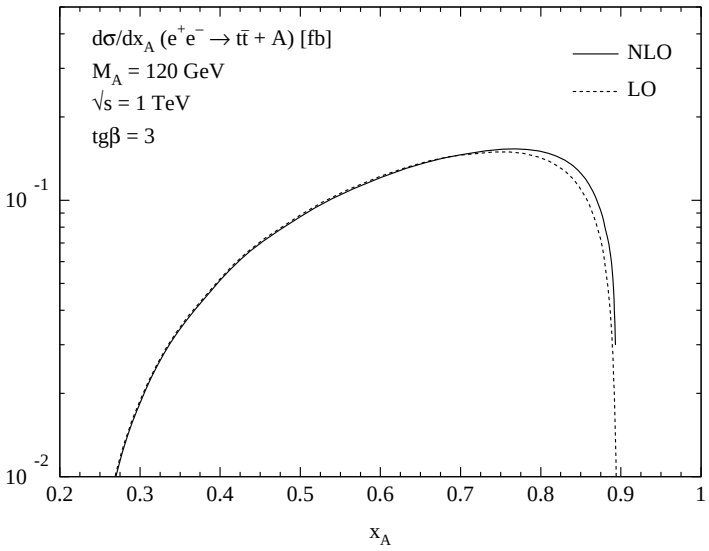

Figure 5: *The Higgs-energy distribution for the process $e^+e^- \to t\bar{t}A + X$, including QCD radiative corrections (full curve) and at LO (dashed curve) as a function of the scaled Higgs energy x_A for $M_A = 120$ GeV at $\sqrt{s} = 1$ TeV [9].*

exemplified in Fig. 6 and for $b\bar{b}A$ production for $M_A = 120$ GeV in Fig. 7 as functions of the corresponding scaled Higgs energies for $\mathrm{tg}\beta = 30$ at $\sqrt{s} = 500$ GeV [9]. The resonance peaks of $A, Z \to b\bar{b}$ are dominating the distribution of $b\bar{b}h$ production and of $h, H \to b\bar{b}$ the distribution of $b\bar{b}A$ production. The continuum contributions are suppressed by several orders of magnitude. The QCD corrections are moderate for all Higgs energies.

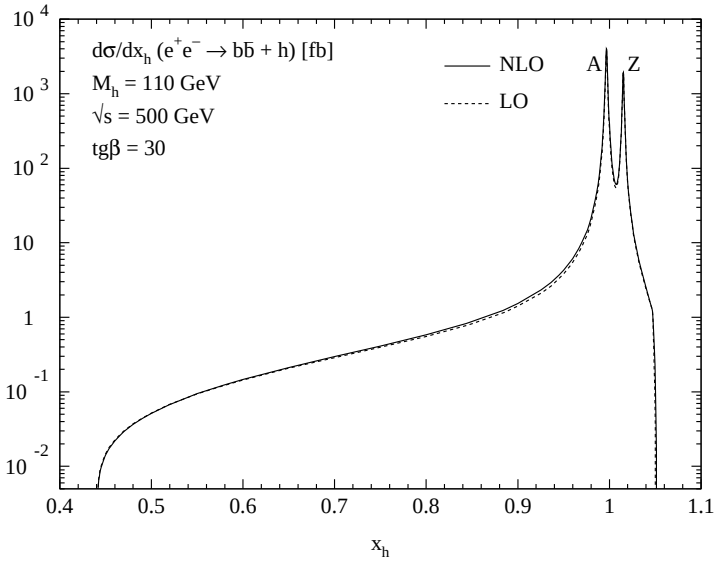

Figure 6: *The Higgs-energy distribution for the process $e^+e^- \to b\bar{b}h + X$, including QCD radiative corrections (full curve) and at LO (dashed curve) as a function of the scaled Higgs energy x_h for $M_h = 110$ GeV at $\sqrt{s} = 500$ GeV [9].*

4 Conclusions

Top- and bottom-Yukawa couplings in the SM and supersymmetric theories can be measured at future linear e^+e^- colliders in Higgs radiation off top and bottom quarks. We have presented the total cross sections and Higgs-energy distributions including the full NLO QCD corrections. The corrections turn out to be large for Higgs radiation off top quarks at c.m. energies $\sqrt{s} = 500$ GeV, while they are moderate at larger energies. The QCD corrections to Higgs radiation off bottom quarks are moderate after absorbing large logarithms in the running bottom Yukawa couplings.

Measurements of the top Yukawa coupling in SM Higgs radiation off top quarks can be performed quite accurately at the future TESLA collider thanks to the high luminosities. Measurements of Yukawa couplings in supersymmetric Higgs radiation off heavy quarks at e^+e^- linear colliders are difficult. This is a result of the large number of subchannels contributing to the $Q\bar{Q}h/H/A$ final states in supersymmetric theories in general, and the contamination by two-Higgs final states in particular. Nevertheless, the continuum cross sections appear large enough to allow for a solution of this experimental problem as shown in the present analysis. Even though experimental simulations are beyond the scope of this note, it may be concluded from earlier SM analyses that the method will work at

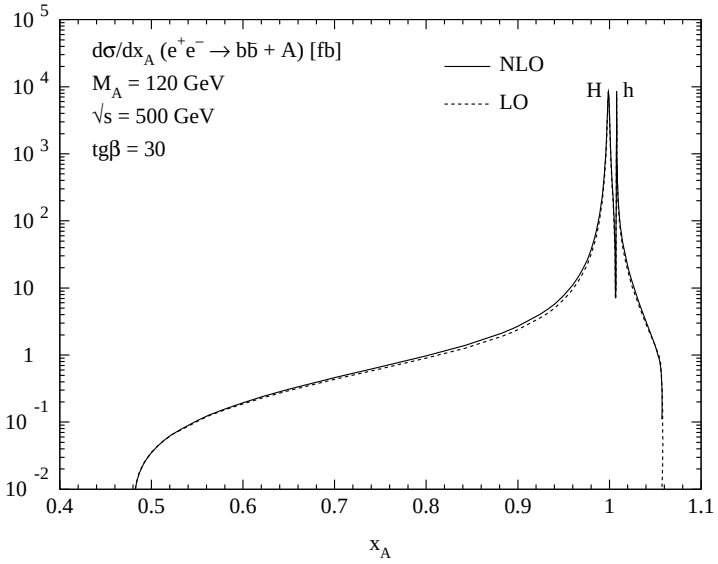

Figure 7: *The Higgs-energy distribution for the process $e^+e^- \to b\bar{b}A + X$, including QCD radiative corrections (full curve) and at LO (dashed curve) as a function of the scaled Higgs energy x_A for $M_A = 120$ GeV at $\sqrt{s} = 500$ GeV [9].*

least in part of the MSSM parameter space, thus providing us with the absolute size of the quark–Higgs Yukawa couplings in the minimal supersymmetric theory.

Acknowledgements. I would like to thank S. Dittmaier, M. Krämer, Y. Liao and P.M. Zerwas for the pleasant collaboration on the topic presented here. Moreover, I am grateful to the organizers of RADCOR–2000 for the stimulating atmosphere during the symposium and financial support.

References

[1] P.W. Higgs, Phys. Lett. **12** (1964) 132; F. Englert and R. Brout, Phys. Rev. Lett. **13** (1964) 321; G.S. Guralnik, C.R. Hagen and T.W. Kibble, Phys. Rev. Lett. **13** (1964) 585.

[2] J.F. Gunion and H.E. Haber, Nucl. Phys. **B272** (1986) 1 and **B278** (1986) 449; J.F. Gunion, H.E. Haber, G.L. Kane and S. Dawson, *The Higgs Hunters Guide*, Addison-Wesley 1990.

[3] P. Fayet and S. Ferrara, Phys. Rep. **32** (1977) 249; H.P. Nilles, Phys. Rep. **110** (1984) 1; H.E. Haber and G.L. Kane, Phys. Rep. **117** (1985) 75; R. Barbieri, Riv. Nuovo Cim. **11** (1988) 1.

[4] M. Spira and P.M. Zerwas, Lectures, 36th Int. Universitätswochen, Schladming 1997, [hep-ph/9803257].

[5] A. Djouadi, J. Kalinowski and P.M. Zerwas, Mod. Phys. Lett. **A7** (1992) 1765 and Z. Phys. **C54** (1992) 255.

[6] A. Juste and G. Merino, Proceedings, Sitges Conference, Barcelona AU Report [hep-ph/9910301]; H. Baer, S. Dawson and L. Reina, Phys. Rev. **D61** (2000) 013002; S. Moretti, Phys. Lett. **B452** (1999) 338; TESLA Collaboration, Technical Design Report, to appear.

[7] S. Dittmaier, M. Krämer, Y. Liao, M. Spira and P.M. Zerwas, Phys. Lett. **B441** (1998) 383.

[8] S. Dittmaier, M. Krämer, Y. Liao, M. Spira and P.M. Zerwas, Phys. Lett. **B478** (2000) 247.

[9] S. Dittmaier, M. Krämer, M. Spira and P.M. Zerwas, in preparation.

[10] C. Caso et al., Particle Data Group, Eur. Phys. J. **C3** (1998) 1.

[11] S. Narison, Phys. Lett. **B341** (1994) 73; M. Jamin and A. Pich, Nucl. Phys. **B507** (1997) 334; M. Beneke and A. Signer, Phys. Lett. **B471** (1999) 233.

[12] M. Carena, H.E. Haber, S. Heinemeyer, W. Hollik, C.E.M. Wagner and G. Weiglein, Nucl. Phys. **B580** (2000) 29, and references therein.

[13] A. Djouadi, J. Kalinowski and P.M. Zerwas, Z. Phys. **C70** (1996) 435.

[14] A. Djouadi, Int. J. Mod. Phys. **A10** (1995) 1; M. Spira, Fortschr. Phys. **46** (1998) 203; A. Djouadi, J. Kalinowski and M. Spira, Comput. Phys. Commun. **108** (1998) 56.

[15] A. Denner, Fortschr. Phys. **41** (1993) 307.

[16] E. Braaten and J.P. Leveille, Phys. Rev. **D22** (1980) 715; M. Drees and K. Hikasa, Phys. Lett. **B240** (1990) 455; (E) **B262** (1991) 497.

[17] S. Dittmaier, Nucl. Phys. **B565** (2000) 69.

[18] A. Djouadi and P. Gambino, Phys. Rev. **D49** (1994) 3499; (E) **D53** (1996) 4111.

[19] S. Dawson and L. Reina, Phys. Rev. **D57** (1998) 5851 and **D59** (1999) 054012.

[20] S. Dawson and L. Reina, Phys. Rev. **D60** (1999) 015003.

[21] W. Beenakker, R. Höpker, M. Spira and P.M. Zerwas, Nucl. Phys. **B492** (1997) 51.